Cyanine Dye N744 Inhibits Tau Fibrillization by Blocking Filament Extension: Implications for the Treatment of Tauopathic Neurodegenerative Diseases†

Mihaela Necula,‡ Carmen N. Chirita,‡ and Jeff Kuret*,§

Biophysics Program, Department of Molecular and Cellular Biochemistry, and Center for Molecular Neurobiology, The Ohio State University College of Medicine, Columbus, Ohio 43210

Received March 1, 2005; Revised Manuscript Received May 27, 2005

ABSTRACT: Tau fibrillization is a potential therapeutic target for Alzheimer's and other neurodegenerative diseases. Small molecules capable of both inhibiting aggregation and promoting filament disaggregation have been discovered, but knowledge of their mechanism of action and potential for testing in biological models is fragmentary. To clarify these issues, the interaction between a small-molecule inhibitor of tau fibrillization, 3,3′-bis(β-hydroxyethyl)-9-ethyl-5,5′-dimethoxythiacarbocyanine iodide (N744), and full-length four-repeat tau protein was characterized in vitro using transmission electron microscopy and fluorescence spectroscopy. Analysis of reaction time courses performed in the presence of anionic fibrillization inducers revealed that increasing concentrations of N744 decreased the total filament length without modulating lag time, indicating that filament extension but not nucleation was affected by inhibitor under the conditions that were investigated. Critical concentration measurements confirmed that N744 shifted equilibria at filament ends away from the fibrillized state, resulting in endwise filament disaggregation when it was added to synthetic filaments. Both increasing bulk tau concentrations and filament stabilizing modifications such as pseudophosphorylation and glycation antagonized N744 activity. The results illustrate the importance of mechanism for the design and interpretation of pharmacological studies in biological models of tau aggregation.

Alzheimer's disease (AD)[1] is diagnosed and staged in part by the appearance of tau-bearing lesions in characteristic regions of the brain (*1*). Lesion-associated tau differs from normal tau in primary structure, being posttranslationally modified, in secondary structure, adopting extensive β-sheet conformation, and in quaternary structure, being organized into filaments with straight and paired-helical morphologies (*2*). Tau-bearing lesions appear in conjunction with neuronal death and cognitive decline (*3*, *4*), suggesting that tau aggregation in some cell populations may directly contribute to disease signs. Tau fibrillization would be an attractive therapeutic target under these circumstances because the formation of ligand binding sites unique to the disease state accompanies its appearance.

To examine the feasibility of this strategy, small-molecule libraries have been screened in search of fibrillization antagonists (*5*−*7*). Multiple classes of inhibitors have been discovered, with especially potent antagonist activity found for members of the cyanine dye family. One of these, N744, has been characterized in detail (*5*). When added to in vitro aggregation reaction mixtures, N744 yields a dose-dependent decrease in filament numbers and mass at the reaction plateau with an IC_{50} more than 1 order of magnitude below bulk tau concentrations. Thus, N744 acts substoichiometrically with respect to tau. N744 also drives the endwise disaggregation of synthetic filaments prepared from full-length recombinant tau isoforms, suggesting it modulates equilibria at filament ends.

Whether this pharmacodynamic spectrum is appropriate for modulating aggregation in the disease state depends on the mechanism of inhibitor action and the fidelity of the in vitro models on which it is based. The latter typically employ purified recombinant tau isoforms and exogenous inducers such as anionic surfactant micelles (*8*, *9*), lipid vesicles (*10*), microspheres (*10*), or polyanions (*11*−*13*) to accelerate the reaction so that it is detectable over tractable time periods (*14*). Inducer-mediated fibrillization proceeds through a heterogeneous nucleation mechanism (*15*), where the interaction of tau with anionic surfaces overcomes the energy barrier to spontaneous filament formation. Under near-physiological conditions of pH, ionic strength, full-length tau concentration, and reducing environment, tau filaments appear on anionic surfaces with Poisson frequency (*16*), suggesting that nucleation events are random, noninteracting, and dependent on the number of nucleating bodies (i.e., micelles, vesicles, etc.) in solution. Growth of the filament population follows nucleation-dependent kinetics, characterized by a lag phase, during which nucleation occurs, an exponential growth phase, during which filament extension dominates, and a plateau

† This work was supported by grants (to J.K.) from the National Institutes of Health (AG14452) and by an Ohio State University Presidential Fellowship (to C.N.C.).

* To whom correspondence should be addressed: OSU Center for Biotechnology, 1060 Carmack Rd., Columbus, OH 43210. Telephone: (614) 688-5899. Fax: (614) 292-5379. E-mail: kuret.3@osu.edu.

‡ Biophysics Program.

§ Department of Molecular and Cellular Biochemistry and Center for Molecular Neurobiology.

[1] Abbreviations: AD, Alzheimer's disease; $C_{18}H_{37}SO_4Na$, sodium octadecyl sulfate; DMSO, dimethyl sulfoxide; N744, 3,3′-bis(β-hydroxyethyl)-9-ethyl-5,5′-dimethoxythiacarbocyanine iodide; PHF, paired-helical filament; ThS, thioflavin S.

10.1021/bi050387o CCC: $30.25
Published on Web 07/07/2005

phase, when the rates of protomer association to and dissociation from filament ends balance each other (*10*, *16*). The balance between association and dissociation reactions is reflected in the "critical concentration" and can be quantified as the highest protein monomer concentration that does not support fibrillization (*17*). Whether the inducer is a long chain fatty acid, alkyl sulfate detergent, or carboxylate-modified microsphere, the reaction plateau is reached after incubation for <24 h, at which time filament morphology and mass-per-unit length correspond to one hemifilament of authentic PHF (*18*, *19*). For this morphology, the equilibrium at filament ends attained in the plateau phase as reflected in critical concentration is independent of inducer structure (*16*, *20*, *21*). In contrast to filament extension, the rate of filament nucleation as reflected in lag times and filament length distributions depends in part on the number of nucleating particles in solution and therefore the structure and concentration of the inducer (*9*, *10*).

Although the model described above is useful for investigating the mechanism of candidate fibrillization inhibitors, the use of modification-free recombinant tau preparations may be inadequate for fully gauging the inhibitory potential of promising fibrillization ligands. In disease, tau is the target of multiple posttranslational modifications that accumulate during lesion formation, including (but not limited to) phosphorylation and glycation (*22*−*24*). Both modifications reduce net charge which, depending on the sites involved, can lead to lowered filament critical concentrations (*21*). Thus, the modification state of tau may be an important factor in the ability of compounds such as N744 to antagonize tau fibrillization in a biological context.

On the basis of its activity spectrum, we postulated that N744 acted as an antagonist of the anionic inducer, inhibiting both nucleation and extension reactions. Here we test this hypothesis using kinetic analysis in the context of recombinant full-length tau isoform htau40. We also address the issue of posttranslational modification by extending the observations to glycated htau40 and pseudophosphorylation mutant htau40^{T212E}. Results indicate that N744-mediated antagonism of inducer activity is limited to the extension reaction, and is itself antagonized by bulk tau concentration and posttranslational modifications. The implications of these observations for pharmacological testing in biological models of tau lesion formation are discussed.

EXPERIMENTAL PROCEDURES

Materials. Recombinant His-tagged wild-type htau40, pseudophosphorylation mutant T212E, assembly incompetent double mutant htau40$^{I277P/I308P}$, and both glycated (∼1 mol/mol stoichiometry) and nonglycated double mutant htau40$^{C291A/C322A}$ were prepared as described previously (*21*, *25*). Stock solutions of alkyl sulfate inducer $C_{18}H_{37}SO_4Na$ (Research Plus, Bayonne, NJ) were prepared in a 1:1 H_2O/2-propanol mixture. Glutaraldehyde, uranyl acetate, and 300 mesh carbon-coated copper grids were from Electron Microscopy Sciences (Ft. Washington, PA). Stock solutions of N744 (deCODE Genetics, Lemont, IL) and ThS (Sigma, St. Louis, MO) were prepared in DMSO and water, respectively. Although ThS is an impure substance (*26*), solutions of it were prepared assuming a molecular mass of 440 Da. Carboxylate-conjugated polystyrene microspheres (90 nm diameter, molecular area of 12 Å^2/equiv) were from Bangs Laboratories, Inc. (Fishers, IN).

Fibrillization Assays. Under standard conditions, tau preparations were incubated without agitation in assembly buffer [10 mM HEPES (pH 7.4), 100 mM NaCl, and 5 mM dithiothreitol] for up to 24 h in the presence or absence of fibrillization inducers ($C_{18}H_{37}SO_4Na$ or carboxylated microspheres). The DMSO vehicle concentration was kept at ≤5% in all reaction mixtures. For analysis by EM, aliquots were removed, treated with 2% glutaraldehyde (final concentration), mounted on Formvar/carbon-coated 300 mesh grids, and negatively stained with 2% uranyl acetate as described previously (*27*). The interfacial filament concentration (Γ_f) is defined as the summed lengths of all filaments >50 nm in length per unit area of grid surface, and is reported in units of length per field ± the standard deviation or as a percentage of wild-type htau40 control values ± the standard deviation.

Right-angle laser light scattering (LLS) assays were performed as described previously (*28*), with the contribution of micellization to scattering intensity controlled by parallel reaction mixtures containing htau40$^{I277P/I308P}$, an assembly incompetent mutant of htau40 (*20*). Net scattering intensities collected at a 90° scattering angle, $I_n(90°)$, are directly proportional to Γ_f values determined by the electron microscopy assay (*20*).

Critical Concentration Determination. Tau samples (3−8 μM, final concentrations) were added from serially diluted stocks to assembly buffer at room temperature and incubated for 26 h in the presence of 50 μM anionic surfactant $C_{18}H_{37}SO_4Na$ and in the absence of agitation, and then analyzed by laser light scattering as described previously (*20*). The net intensity of scattered light corresponding to fibrillization was plotted against tau concentration. The critical concentration was estimated from the abscissa intercept.

ThS Fluorescence Measurements. Tau was aggregated at 37 °C as described above except that the reaction mixtures contained 2−40 μM ThS and varying concentrations of N744 (0−4 μM). The time course of resultant changes in fluorescence was monitored at a λ_{ex} of 440 nm and a λ_{em} of 495 nm in a FlexStation plate reader (Molecular Devices, Sunnyvale, CA) operated at sensitivity 10, high PMT using black-matrix, clear-bottom 96-well isoplates (Wallac, Turku, Finland) sealed with transparent foil (NUNC). Initial velocities and plateau levels of fluorescence were estimated by fitting time courses to sixth-power polynomials and rectangular hyperbolas, respectively, as described previously (*10*).

Dye Aggregation. N744 (0.25−5 μM, total concentration) was incubated (37 °C for 2 h) in assembly buffer (containing 5 mM DTT) and then subjected to absorbance scans (450−650 nm). Concentrations of dye monomer (C_m) were estimated as described by West and Pearce (*29*). Briefly, the extinction coefficient for the N744 monomer was established in methanol ($\epsilon_{560} = 1.36 \times 10^5$ M^{-1} cm^{-1}) and then used to estimate the monomer concentration in aqueous solutions after deconvoluting absorbance data with a triple-Gaussian function. The N744 dimer concentration (C_d) was estimated from the total dye concentration (C) and the assumption (*29*)

$$C_d = (C - C_m)/2 \quad (1)$$

The dissociation constant for dimerization (K_{dim}) was then

calculated from the function (*29*)

$$K_{dim} = C_m^2/C_d \quad (2)$$

Thus, the slope of double log plots of C_m versus C_d was taken as an indicator of reaction order (i.e., dimerization), whereas the ordinate intercept was taken as K_{dim}.

Analytical Methods. Sigmoidal fibrillization progress curves were fit to a three-parameter Gompertz function as described previously (*20*). Lag times, defined as the time when the tangent to the point of maximum polymerization rate intersects the abscissa of the sigmoidal curve (*30*), were calculated from the resultant Gompertz parameters (*20*).

Concentration response curves for aggregation and disaggregation were fit to the function

$$y = y_{min} + \frac{y_{max} - y_{min}}{1 + 10^{(\log IC_{50} - \log x)n}} \quad (3)$$

where y and y_{max} are the total filament lengths measured in the presence and absence of inhibitor (at concentration x), respectively, and n is the Hill coefficient. Measurements were normalized so that y_{max} was always defined as 100%, whereas y_{min}, the total filament length remaining when inhibitor concentrations were extrapolated to saturation, was not constrained.

The EC_{50} for ThS fluorescence (defined as the concentration of ThS probe required to produce half-maximal initial velocity or plateau fluorescence) was estimated from the abscissa intercepts of double-reciprocal plots analyzed at varying N744 concentrations.

Cooperativity of N744 competition was assessed using Hill plots of the form

$$\log \frac{y}{1-y} = -n \log[\text{N744}] + \log IC_{50} \quad (4)$$

where y is the fluorescence in the presence of N744 expressed as a fraction of the fluorescence recorded in the absence of N744 and n is the Hill coefficient (a measure of cooperativity).

The K_i for N744 binding was estimated using a Schild plot modified to include the contribution of inhibitor cooperativity (*31*):

$$\log(EC_{50}\ \text{ratio} - 1) = \log[\text{N744}]^n - \log K_i \quad (5)$$

with parameters determined as described above.

All parameters estimated by linear or nonlinear regression are reported with the standard error.

RESULTS

Kinetic Analysis of N744 Activity. To determine the effects of N744 on tau aggregation kinetics, the time course of htau40 fibrillization was examined in the presence of the anionic microsphere inducer under standard, near-physiological conditions of pH, ionic strength, bulk tau concentration (4 μM), and reducing conditions. Microspheres were chosen as the inducer because, unlike anionic surfactants, they do not undergo micellization or otherwise change structure during reaction time courses that can affect lag time (*10*). In the absence of N744, tau formed filaments with nucleation-dependent kinetics, characterized by lag, exponential growth, and plateau phases (Figure 1A). Consistent with previous results (*5*), increasing concentrations of N744 led to decreases in total filament length remaining at 24 h [i.e., reaction plateau (Figure 1A)]. The maximum growth rate, corresponding to the slope at the point of inflection, also decreased with increasing N744 concentrations (Figure 1A). In contrast, N744 had little effect on fibrillization lag times (Figure 1B). Because lag times depend in part on nucleation rates (*32*), these data indicate that N744 did not inhibit filament nucleation. Rather, N744 selectively inhibited the extension phase of fibrillization, leading to slower growth rates for the filament population and decreased total filament length (i.e., total filament mass) at the reaction plateau.

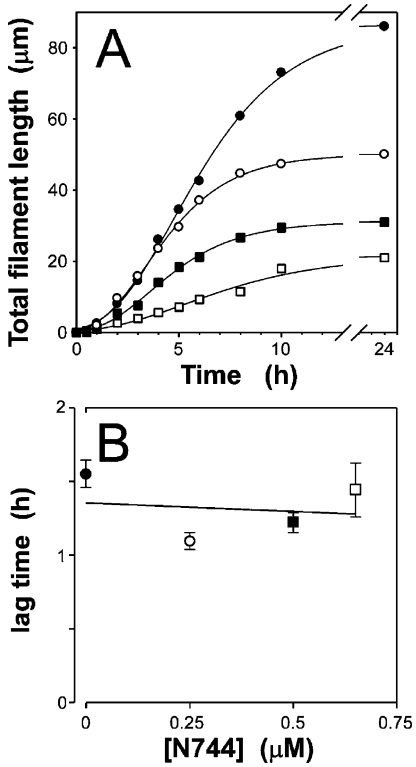

FIGURE 1: Effect of N744 on tau fibrillization kinetics. (A) Fibrillization of wild-type htau40 (4 μM) in the presence of a carboxylate-substituted polystyrene microsphere inducer (90 nm diameter, 12 Å^2/equiv molecular area; 124 pM) was assayed as a function of incubation time and N744 concentration at room temperature. Each data point [(●) 0, (○) 0.25, (■) 0.5, and (□) 0.65 μM N744] represents total filament lengths calculated from electron micrographs (mean of duplicate determinations), whereas each curve represents the best fit of the data points to a three-parameter Gompertz growth function. The presence of N744 led to decreases in total filament lengths at the reaction plateau. (B) Values for lag time were calculated from data in panel A and replotted vs N744 concentration. N744 yielded concentration-dependent decreases in the level of plateau fibrillization but not lag time.

N744 Modulates the Critical Concentration. To test this hypothesis, the critical concentration of htau40 fibrillization was determined in the presence of varying N744 concentrations using a corrected laser light scattering assay (*20*). The critical concentration corresponds to the maximal solubility of the protein above which all additional assembly competent protein enters the polymeric phase, and for a nucleation−elongation mechanism, the critical concentration approximates the equilibrium constant for filament extension (*33*).

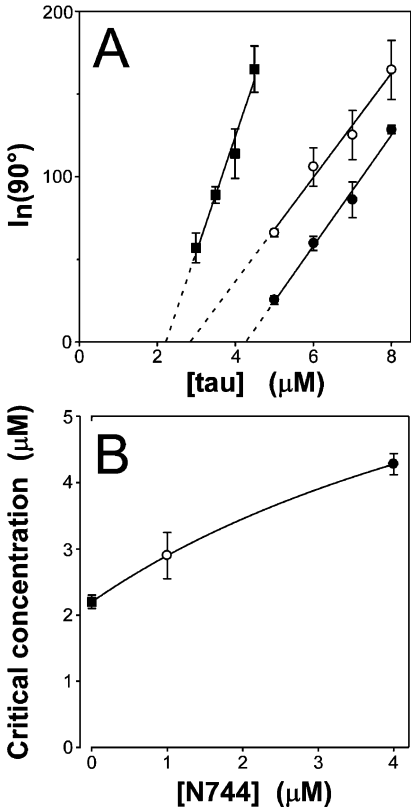

FIGURE 2: Effect of N744 on the critical concentration of assembly. (A) The fibrillization of wild-type htau40 incubated (room temperature for 26 h) with the $C_{18}H_{37}SO_4Na$ inducer (50 μM) in assembly buffer was assayed as a function of N744 [(■) 0, (○) 1, and (●) 4 μM] tau concentration (3−8 μM) by static laser light scattering. Each data point represents the average (±standard deviation; $n = 4$) net intensity of scattered light, $I_n(90°)$, at a specific tau concentration, whereas each solid line represents linear regression analysis of the data points. The critical concentration of assembly (estimated from the abscissa intercept of each regression line) was dependent on N744 concentration. (B) Replot of data in panel A, where each point corresponds to the critical concentration as a function of N744 (±the standard error of the regression fit), whereas the solid line is drawn solely to aid visualization. The critical concentration increases with increasing concentrations of N744.

It is the highest protein concentration that does not support fibrillization, and therefore can be estimated from the dependence of fibrillization on bulk protein concentration (*17*). $C_{18}H_{37}SO_4Na$ was chosen as the inducer for this experiment because it supports fibrillization with the same critical concentration as anionic microspheres but is amenable to light scattering techniques (*20*). The critical concentration for wild-type htau40 in the presence of the $C_{18}H_{37}SO_4Na$ inducer and DMSO vehicle under standard assembly conditions was 2.2 ± 0.2 μM (Figure 2A). The presence of N744 shifted the curves relating light scattering intensity to tau concentration to the right (Figure 2A), indicating that the critical concentration was dependent on N744 concentration. Indeed, replots of critical concentration versus N744 concentration indicated that the former steadily increased with N744 concentration (Figure 2B). These data confirm that the decreased level of fibrillization observed in the presence of N744 resulted from changes in equilibria at filament ends. They also reveal that the inhibitory effects of N744 on plateau filament length could be overcome by increasing bulk tau concentrations (Figure 2A).

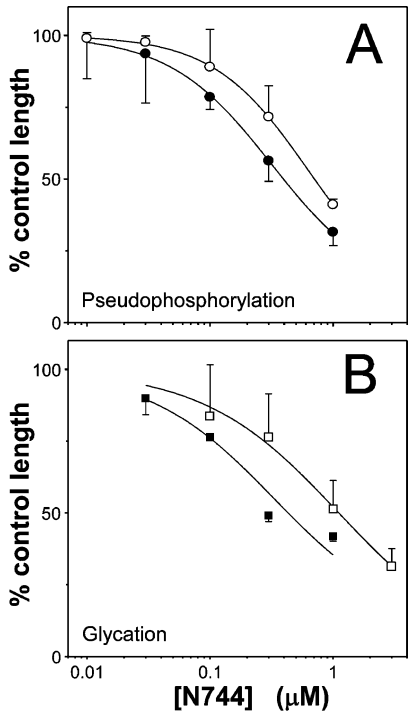

FIGURE 3: N744 action is antagonized by posttranslational modifications. (A) Wild-type htau40 (●) and pseudophosphorylation mutant htau40^{T212E} (○) and (B) nonglycated (■) and glycated (□) htau40$^{C291A/C322A}$ were each incubated (5 h at 22 °C) at 4 μM with the $C_{18}H_{37}SO_4Na$ inducer (50 μM) in assembly buffer and various concentrations of N744 in DMSO without agitation. Aliquots were then removed, stained with uranyl acetate, and viewed in a transmission electron microscope as described in Experimental Procedures. Each point represents the total length of all filaments expressed as a normalized percentage of filament lengths measured in the absence of N744 (triplicate determination ± the standard deviation), whereas the curve represents the best fit of the data points to eq 3. Under these conditions, N744 inhibitory potency was attenuated by both pseudophosphorylation and glycation.

Effect of Posttranslational Modification. Unlike recombinant preparations, tissue-derived tau contains posttranslational modifications that can modulate aggregation behavior. For example, both pseudophosphorylation and glycation of htau40 lead to decreases in critical concentration (*21*). Thus, modifications such as these are predicted to antagonize the activity of N744. To test this hypothesis, concentration response curves were prepared for both wild-type htau40 and pseudophosphorylation mutant htau40^{T212E} in the presence of the $C_{18}H_{37}SO_4Na$ inducer. The latter preparation was chosen for analysis because it returns the largest change in critical concentration of any phosphorylation mimicry mutant studied to date, thereby ensuring that any differences in N744 potency would be large enough to measure. Moreover, it binds N744 with an affinity similar to that of htau40 (*34*), eliminating differences in binding affinity as a variable. When N744 was present under standard conditions, the IC_{50} for N744 inhibition of htau40 fibrillization at 24 h was 280 ± 20 nM (Figure 3). In contrast, the IC_{50} for pseudophosphorylation mutant htau40^{T212E} treated under identical conditions was 630 ± 20 nM (Figure 3). These data confirm that N744 potency is sensitive to modifications that modulate equilibria at filament ends. To extend the analysis to glycation, the fibrillization of glycated and nonglycated htau40$^{C291A/C322A}$ was examined in the presence and absence of N744. The C291A/C322A mutant was used for this

experiment because it eliminated potential complications arising from cysteine oxidation during the glycation reaction (*21*). IC_{50} values for N744-mediated inhibition of nonglycated and glycated htau40$^{C291A/C322A}$ fibrillization were 420 ± 310 nM and 1.3 ± 0.6 μM, respectively (Figure 3). Again, the differential sensitivity to N744 did not arise from differences in N744 binding affinity (data not shown). Together, these data predict that posttranslational modifications, such as those that accompany tau fibrillization in vivo, can influence the potency of fibrillization inhibitors and potentially antagonize their activity.

N744 Binds Competitively with ThS. The submicromolar potency of N744 against recombinant full-length htau40 suggests that it binds one or more sites with prearranged structure. In fact, the planar aromatic nature of the dye indicates that these may be the same β-sheet-containing sites bound by fluorescent reporter dyes such as ThS. To test this hypothesis, the ability of N744 (0−4 μM) to compete with ThS binding (2−40 μM) was determined using fluorescence spectroscopy in the presence of anionic microspheres. This inducer yields slow aggregation kinetics and so is ideal for measurement of initial rates (*16*). In the absence of N744, ThS bound tau species with an apparent EC_{50} of 11 ± 2 μM on the basis of double-reciprocal plots of initial velocity of fluorescence development versus ThS concentration (Figure 4A). Increasing concentrations of N744 yielded a family of lines with common ordinate intercepts, consistent with it acting as a competitive inhibitor of ThS binding. This pattern held for both initial velocity and plateau levels of fluorescence. However, replots of double-reciprocal plot slopes versus N744 concentration were parabolic (data not shown), suggesting that the interaction of N744 with tau species was cooperative, and precluding estimation of K_i by this method.

To assess cooperativity, concentration response curves were plotted in Hill plot format, yielding a family of parallel lines that shifted toward higher IC_{50} values with increasing concentrations of the ThS probe (Figure 4B). The overall pattern was again consistent with competitive inhibition at every tested concentration of probe and inhibitor. The Hill coefficient averaged 1.4 ± 0.1 (n = 5 curves), indicating the presence of positive cooperativity.

In cooperative competitive binding reactions, K_i can be estimated from the ordinate intercepts of Schild plots modified to include effects of positive cooperativity (*31*). Although the precise molar concentration of ThS is unknown in these experiments, derivation of K_i values for competitive binding depends on probe concentration relative to its EC_{50} rather than to its absolute concentration and K_D (*35*). Using this approach, a K_i value for N744 of 170 ± 10 nM was determined (Figure 4C). Together, these data confirm that the binding affinity of N744 is substoichiometric with respect to bulk tau concentrations and that its binding site consisted of the same β-sheet-containing elements bound by ThS.

N744 Forms Supramolecular Aggregates. ThS reacts with multiple aggregation reaction products, including partially folded intermediates (*10*) and mature filaments (*36*). Although it is difficult to distinguish multiple binding sites of differing affinity from true cooperativity, the former phenomenon generally resembles negative cooperativity (*37*), whereas both the fibrillization inhibition and competitive binding isotherms for N744 are characterized by positive cooperativity. Positive cooperativity potentially stems from

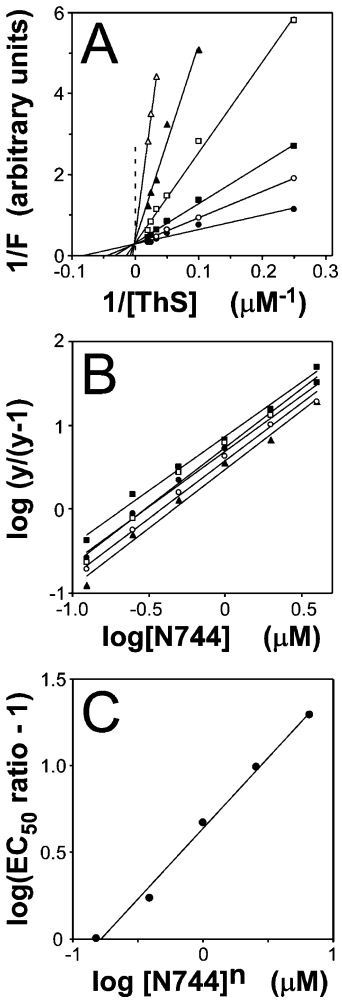

FIGURE 4: N744 binds competitively with ThS. (A) Htau40 (4 μM) was incubated (22 °C) with a carboxylate-substituted polystyrene microsphere inducer (124 pM) in the presence of 2, 4, 10, 20, 30, or 40 μM ThS probe and 0 (●), 0.13 (○), 0.25 (■), 0.5 (□), 1 (▲), and 2.5 μM N744 (△) and then subjected to fluorescence spectroscopy (λ_{ex} = 440 nm; λ_{em} = 495 nm). Double-reciprocal plots of the initial velocity of fluorescence development vs ThS concentration (duplicate determination) show that increasing concentrations of N744 led to increasing ThS EC_{50} values (abscissa intercept) without changes in maximum fluorescence velocity (i.e., the ordinate intercept). The pattern is consistent with N744 acting as a competitive inhibitor of ThS binding. (B) Competitive fluorescence data shown in panel A were replotted in Hill format (eq 4) against varying concentrations of ThS probe [(■) 2, (□) 4, (●) 10, (○) 20, and (▲) 30 μM]. Each solid line represents a best fit to a linear regression. N744 inhibitory activity was cooperative at all ThS concentrations that were investigated, with Hill coefficients averaging 1.4 ± 0.1. The family of shifting parallel lines confirms that N744 competes with ThS binding under these conditions. (C) EC_{50} and Hill coefficients determined from panels A and B, respectively, were replotted in Schild format modified to included inhibitor cooperativity (eq 5) and fit to a linear regression. On the basis of the abscissa intercept, the K_i for competitive N744 binding was 170 ± 10 nM.

allosteric transitions, where the binding energy of one ligand influences the binding of another by stabilizing conformational changes in the protein, or by the creation of more favorable binding sites for subsequent ligands via direct ligand−ligand interactions (*38*). With respect to the latter mechanism, thiacarbocyanine derivatives are known to self-associate both in aqueous solution and on solid surfaces because of strong dispersion forces between their nearly

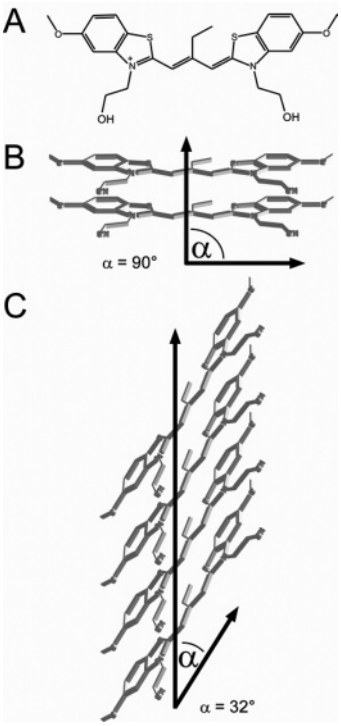

FIGURE 5: Hypothetical structures for N744 aggregates. N744 is a symmetrical thiacarbocyanine derivative consisting of two heterocyclic rings containing nitrogen atoms linked by a conjugated methine bridge. Dyes of this class form aggregates in aqueous solution with H- or J-type absorbance character depending on the angle of slippage (α) between successive molecular planes (α defines the angle between the line of centers of a column of dye molecules and the long axis of any constituent molecule), with small slippage angles (α < ∼32°) resulting in bathochromic shifts (i.e., J-bands) and large slippage angles (α > ∼32°) resulting in hypsochromic shifts (i.e., H-bands). (A) Monomeric structure predominates in methanolic solution. (B) Hypothetical structure of N744 in H-dimer aggregation state. (C) Hypothetical N744 tetramer for which α = 32°. H- and J-aggregates are characterized by slippage angles of greater than and less than 32°, respectively.

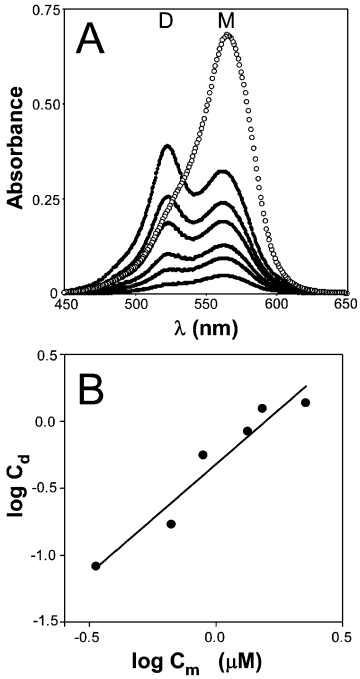

FIGURE 6: N744 absorption spectra. (A) N744 (5 μM) in methanol (○) exhibits a single peak consistent with monomeric structure. In assembly buffer (solid lines), increasing concentrations of N744 (0.5, 1, 2, 3, 4, and 5 μM) revealed the presence of both monomeric (M) and dimeric (D) species, with the latter more pronounced as bulk N744 concentrations increase. (B) Concentrations of monomer (C_m) and dimer (C_d) calculated from data in panel A were replotted against each other on a double logarithmic scale and fit to a linear regression. The regression slope was 1.7 ± 0.2, consistent with N744 undergoing a dimerization reaction. The dissociation equilibrium constant for dimerization (K_{dim}) was 2.1 ± 0.4 μM.

planar faces (*39*). Shifts in absorbance spectra accompany thiacarbocyanine aggregation depending on the quaternary structure of the aggregate that is formed. Hypsochromic shifts to shorter wavelengths are generally called H-bands. In solution, these correspond primarily to small aggregates (dimer, trimer, etc.), but much larger sizes can be attained especially when they are grown on solid substrates (*40*). Bathochromic shifts to longer wavelengths are termed J-bands. These correspond to large aggregates that at high concentrations in solution can achieve a liquid crystal state (*41*). Although both classes of aggregates are composed of parallel dye molecules stacked plane to plane, they differ in the angle of slippage (α) between successive molecular planes (Figure 5).

To determine whether N744 aggregated in solution, its absorbance spectrum was measured as a function of concentration. In neat methanol, which does not support dye oligomerization (*29*), N744 absorbance appeared as a major band at 568 nm with a weak vibrational shoulder at 547 nm (Figure 6A). At low micromolar concentrations in aqueous solution (i.e., assembly buffer), the monomer appeared to be centered at 562 nm, consistent with the solvatochromic behavior of many thiacarbocyanine derivatives (*42*). As N744 concentrations increased, a second maximum centered at 522 nm also became apparent. On the basis of absorption spectra of other thiacarbocyanine dyes (*29*), the 522 nm band corresponds to an H-dimer of N744 (Figure 5). To confirm this prediction, the amount of monomer as a function of bulk N744 concentration was determined by absorbance spectroscopy and used to calculate the concentration of putative dimer using eq 1. A double log plot of monomer versus dimer concentration was linear with a slope of 1.7 ± 0.2, confirming that the reaction was consistent with dimerization (Figure 6B). On the basis of the ordinate intercept of this plot, the dissociation equilibrium constant for dimerization (K_{dim}) was 2.1 ± 0.4 μM. These data demonstrate that N744 readily dimerizes at low micromolar concentrations under near-physiological buffer conditions.

Cyanine dye aggregation is sensitive to the presence of binding substrate, including proteins with varying secondary structure (*43*−*46*). To determine whether β-sheet-containing tau species affected N744 aggregation, htau40 pretreated with the $C_{18}H_{37}SO_4Na$ inducer in assembly buffer was exposed to N744 and the resultant absorbance pattern measured after incubations for 0 and 30 min. These conditions lead to formation of inducer micelles (*9*), which interact with tau and stabilize tau β-structure (*16*). Because micelles could complicate the absorbance pattern of N744, parallel reaction mixtures were prepared by replacing tau with mixed histones, a protein preparation that induces surfactant micellization but that does not fibrillize under these conditions (*20*). Histone concentrations were chosen on the basis of Corrin−Harkins plots (*10*) to yield similar amounts of micelles as tau protein (*20*). Thus, the histone-containing reaction served

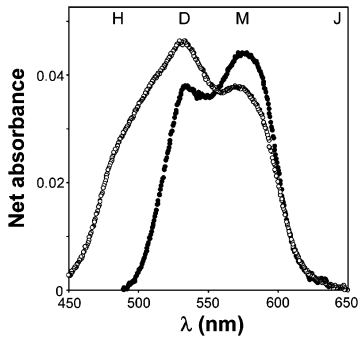

FIGURE 7: N744 forms H-aggregates in the presence of tau filaments. Fibrillization inducer $C_{18}H_{37}SO_4Na$ (50 μM) was incubated (2 h at 22 °C) in assembly buffer containing either 4 μM htau40 or 0.6 μM mixed histones. Aliquots of each reaction mixture were then brought to 4 μM N744 (final concentration) and subjected to absorption spectroscopy. Difference spectra ($A_{htau40} - A_{histone}$) calculated immediately after N744 addition (●) show that the tau sample bound both monomeric (M) and dimeric (D) species but not higher-order H- or J-aggregates. In contrast, a 30 min incubation (○) led to substantial aggregation of N744 into both dimer and H-aggregate forms. These data indicate that N744 can oligomerize in the presence of tau filaments and partially folded intermediates.

as a control for nonspecific, micelle-associated changes in N744 absorbance. Difference spectra between tau and histone reactions are shown in Figure 7. Immediately after N744 had been added, the difference spectrum showed the presence of both H-dimer and monomer peaks in the tau sample with the latter predominating. After incubation for a further 30 min, however, the pattern evolved so that dimer predominated over monomer. In addition, a broad shoulder appeared at wavelengths of ≤500 nm, consistent with the formation of higher-order H-aggregates (Figure 7). Together, these data indicate that N744 is prone to aggregation in aqueous solution, that both dimers and higher-order oligomers form complexes with tau under fibrillization conditions, and that dye aggregation is a potential source of positive cooperativity in competitive binding and activity assays.

DISCUSSION

Mechanism. N744 inhibits tau fibrillization cooperatively with respect to N744 concentration and substoichiometrically with respect to bulk tau concentration, yielding fewer filaments of shorter length at reaction plateau than vehicle-only controls (*5*). N744 also promotes the disaggregation of mature synthetic filaments. On the basis of this pattern, it was predicted that N744 was an antagonist of the inducer, potentially interfering with both nucleation and extension phases of assembly (*5*). Anionic inducers present surfaces that bind free tau and shift the equilibrium of monomer conformations toward assembly competent states (*9*; Figure 8). These are characterized in part by partially folded, β-sheet-enriched structures that can be detected through their ability to bind ThS (*10*, *16*). Assembly competent species self-associate on anionic surfaces to form oligomeric nuclei (*47*). The unfavorable nucleation reaction may correspond to interactions orthogonal to the nascent filament axis unrelated to β-sheet formation (*48*). Free tau then adds to nascent filament ends to extend the β-sheet structure parallel to the axis of the fiber and perpendicular to the inducer surface (Figure 8). A similar morphological relationship between tau filaments and membranes has been observed in biopsy specimens of AD tissue (*49*), suggesting this general sequence of events (i.e., heterogeneous nucleation) may be pathophysiologically significant. At a minimum, therefore, micellar anionic inducers modulate tau conformational equilibria to trigger nucleation. They may also act catalytically (*50*) by increasing the concentration of assembly competent species free in solution (i.e., not micelle-associated).

The results presented here suggest that N744 does not antagonize the triggering aspects of anionic surfactant inducer action. Rather, its inhibitory activity stems primarily from interference with equilibria at filament ends as indicated by its dose-dependent modulation of filament critical concentration. Thus, addition of N744 to aggregation reaction mixtures results in decreased filament length at reaction plateau without changes in nucleation rate as inferred from lag time measurements. As a result, length distributions shift toward shorter lengths as extension rates decrease relative to nucleation rates. When N744 is added to mature filaments, the resultant increase in critical concentration results in endwise depolymerization (*5*). The disaggregation reaction proceeds with pseudo-first-order kinetics at early time points because initial movement to the new equilibrium is controlled by the rate of dissociation from filament ends and the starting length distribution is near-exponential (*34*).

Together, these data predict that N744 inhibits tau fibrillization either indirectly by sequestering the tau protomer or directly by decreasing the rates of association and/or increasing rates of dissociation from filament ends. Examples of the former have been reported under nonreducing conditions. Intramolecular disulfide bond formation can trap four-repeat tau isoforms in assembly incompetent conformations (*51*, *52*). Similarly, some compounds can form covalent adducts

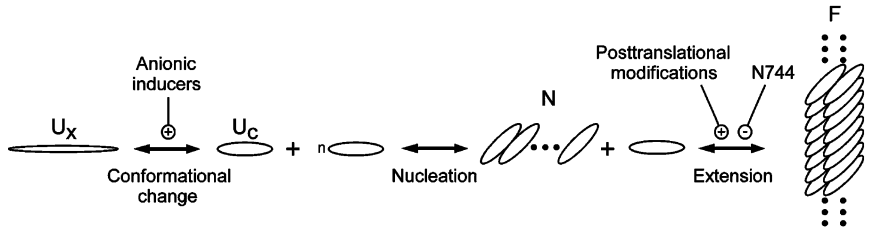

FIGURE 8: Hypothetical scheme for tau aggregation in vitro. Under reducing conditions, tau is a natively unfolded monomer (U_x) that is assembly incompetent. The presence of anionic inducers stabilizes assembly competent conformations (U_c) that can aggregate through a nucleation−elongation mechanism. The nucleus (N) corresponds to an essential but scarce cluster of molecules that reacts efficiently with assembly competent conformations of free tau in an extension reaction to form filaments with the mass-per-unit length of PHF hemifilaments (F). N744 directly or indirectly interferes with the extension reaction, suggesting it inhibits association with and/or accelerates dissociation from filament ends. N744 also antagonizes the extension promoting activity of posttranslational modifications such as pseudophosphorylation and glycation. See the Discussion for details.

(e.g., Schiff base) with filament-forming proteins, potentially trapping them as assembly incompetent monomers (*53*) or oligomeric complexes (*54*). Protomer sequestration yields lower effective monomer concentrations, leading to increased lag times for homogeneous nucleation and destabilization of mature filaments (*53*−*55*). The latter phenomenon can appear as an increase in the apparent critical concentration. Covalent protomer sequestration may mediate the inhibitory activity of anthraquinones in tau fibrillization, and may account for the dependence of inhibitory potency on reaction redox conditions (*6*). The principal argument against N744 acting in this way is its failure to inhibit the nucleation rate as reflected in lag time measurements. These negative data must be interpreted with caution, however, because tau fibrillization was investigated under heterogeneous nucleation conditions, the rate of which depends on the number of nucleating particles in solution as well as supersaturation (*15*). It is conceivable that a decreased level of supersaturation secondary to tau sequestration leads to slower nucleation rates that are detectable in homogeneous nucleation regimes, but not under the heterogeneous nucleation conditions employed in this study.

In terms of direct action, the substoichiometric binding and inhibitory activities of N744 suggest that its binding site is present at low concentrations and corresponds to only a portion of bulk tau in the reaction. But identifying those species in the context of the proposed assembly pathway (Figure 8) is complicated by the lack of knowledge of their relative concentrations, affinity for N744 or ThS probe, or relative fluorescence yield when bound with ThS. The presence of anionic inducers leads to the formation of at least three pools of tau, consisting of free tau in solution, tau adsorbed to anionic surfaces, and tau filaments (*10*). As pointed out above, anionic inducers may also act catalytically to build up a pool of assembly competent tau in solution. Because N744 inhibitory activity is expressed at filament ends, either filamentous tau and/or soluble tau in an assembly competent conformation could serve as its binding site.

Dye Structure. Aromatic dyes, including ThS and Congo Red, are popular probes of amyloid conformation because of their ability to bind extended β-sheet structure with high affinity (*56*, *57*). The exact nature of their binding sites is unclear, however, with parallel and orthogonal orientations with respect to the fiber axis being consistent with optical and X-ray crystallographic experiments, respectively (*58*−*60*). Adding more complexity, the dyes bind nonfibrillar β-sheet-containing species, including protein monomers (*10*, *61*, *62*). For the parallel orientation, the minimum requirement for binding may be the number of strands in a β-sheet, being at least four for thioflavin T (*60*). On the basis of its competitive binding pattern, cyanine dye N744 joins ThS in binding these sites; however, thioflavin dyes do not inhibit tau fibrillization under near-physiological assay conditions, whereas cyanine dyes such as N744 inhibit when present at low to sub-micromolar concentrations.

What structural features confer antagonist activity? Many polycyclic compounds aggregate in solution to form H- and J-aggregates (*63*), and these reactions are facilitated by the presence of binding substrates such as proteins. For this reason, aggregation of small molecules has been considered a nuisance in drug screening assays (*64*). For example, anthraquinones form aggregates that inhibit phosphomannomutase/phosphoglucomutase noncompetitively with respect to a carbohydrate substrate (*65*). Cyanine dyes also aggregate but are distinctive in their ability to do so at low concentrations (*66*) and in the presence of macromolecules with organized substructure, including duplex DNA (*67*) and the secondary structure elements of proteins (*44*). In contrast to the interaction between anthraquinones and phosphomannomutase/phosphoglucomutase, the binding of cyanine aggregates to macromolecules can be highly selective. In the case of duplex DNA, cyanine H-aggregates fill the minor groove (*42*, *67*) with binding affinity and selectivity dependent on annular shape (i.e., a shape matching the curvature of the minor groove), van der Waals contacts with the walls of the groove, hydrogen bonding with the edge of pi-stacked bases, and release of ordered water molecules (*68*). Similar forces may mediate the association of N744 aggregates with the ThS binding site on tau, rationalizing the cooperative nature of both dose response and competitive ThS binding data. Structure−activity relationship data will clarify whether dye aggregation behavior can be separated from inhibitory activity.

Pharmacological Potential. N744 and other cyanine dyes may have utility for inhibiting tau aggregation in biological models of tauopathy because they readily cross cell membranes (*69*) and are nontoxic as indicated by the approval of Cardio-green (Food and Drug Administration Application 011525) for use in humans (*70*, *71*). Absorption spectroscopy indicates that dye aggregation can follow binding of target sites, and so may not impose a pharmacokinetic constraint if it proves to be important for inhibitory activity. But the mechanism of inhibition reported here suggests that testing of compounds such as N744 in biological models may be complicated by other factors. First, the critical concentration lowering activity of N744 is antagonized by site-specific incorporation of negative charge, suggesting that physiological posttranslational modifications such as phosphorylation will lower N744 potency. Glycation, which also lowers net charge and critical concentration, also antagonizes N744 action. Second, as shown in Figure 2A, N744 activity is antagonized by bulk tau protein concentrations. Current biological models of tau fibrillization rely on supraphysiological expression levels to empirically drive aggregation (*72*). Intracellular tau concentrations can reach 80 μM in these systems, at least 1 order of magnitude above normal levels (*73*). Models that rely on high-level expression are not representative of the disease state, where the total expression level of all tau isoforms does not markedly increase (*74*, *75*). Thus, an inhibitory mechanism that may hold promise in vivo may be difficult to validate in biological models at least with respect to the sub-micromolar potency seen in vitro with purified recombinant tau preparations. Nonetheless, the data presented here suggest that the effects of both high bulk tau concentrations and posttranslational modifications can be overcome by N744 as long as the elevated concentrations needed to do so are tolerated by the model.

Several pharmacological strategies have been developed for inhibiting protein conformational changes or the toxicity associated with them. First, anionic compounds, including glycosaminoglycan mimetics (*76*) and sulfated aromatic dyes (*77*), may sequester protein to weaken its ability to associate with itself or other molecules. Application of this strategy

to tau protein could be problematic, however. Although depletion of tau over short time periods is well tolerated by some criteria (*78*, *79*), chronic depletion of protomer may have deleterious effects (*80*). A second category includes aromatic dyes that need not be anionic to serve as aggregation inhibitors (*5*, *6*, *81*). These may act by mechanisms other than sequestration, but analyses of inhibitory mechanism have lagged well behind descriptions of composition of matter. For these molecules, inhibitory potency reported on the basis of thioflavin dye fluorescence should be interpreted with caution because of the potential for competitive binding. For example, rates of filament disaggregation in the presence of 4,5-dianilinophthalimide assessed using thioflavin dye fluorescence as probe appear to be extremely rapid (*82*) compared to the time required for endwise dissociation of protomers from amyloid filaments made on the basis of electron microscopy or light scattering measurements (*34*). These data may result from rapid, diffusion-limited antagonism of probe binding rather than filament disaggregation. Third, disaggregation of mature filaments through the use of bifunctional reagents has been demonstrated for intracellular targets (*83*). However, random filament breakage can yield seeds for aggregate formation which may complicate their utility in some cases (*84*). Finally, it is possible to stabilize the native folded state of aggregating proteins so that assembly competent intermediates cannot form efficiently (*85*). Application of this strategy to tau protein is complicated by the lack of tertiary structure in its biologically functional form.

Together, these considerations suggest that inhibition of tau aggregation is challenging but amenable to pharmacological modulation. Inhibitory mechanism has important implications for design and interpretation of pharmacological studies in biological models.

ACKNOWLEDGMENT

We thank Dr. Mike Zhu (The Ohio State University Center for Molecular Neurobiology) for assistance with fluorescence measurements.

REFERENCES

1. Murayama, S., and Saito, Y. (2004) Neuropathological diagnostic criteria for Alzheimer's disease, *Neuropathology 24*, 254−260.
2. Brandt, R., Hundelt, M., and Shahani, N. (2005) Tau alteration and neuronal degeneration in tauopathies: Mechanisms and models, *Biochim. Biophys. Acta 1739*, 331−354.
3. Arriagada, P. V., Growdon, J. H., Hedley-Whyte, E. T., and Hyman, B. T. (1992) Neurofibrillary tangles but not senile plaques parallel duration and severity of Alzheimer's disease, *Neurology 42*, 631−639.
4. Ghoshal, N., Garcia-Sierra, F., Wuu, J., Leurgans, S., Bennett, D. A., Berry, R. W., and Binder, L. I. (2002) Tau conformational changes correspond to impairments of episodic memory in mild cognitive impairment and Alzheimer's disease, *Exp. Neurol. 177*, 475−493.
5. Chirita, C. N., Necula, M., and Kuret, J. (2004) Ligand-dependent inhibition and reversal of tau filament formation, *Biochemistry 43*, 2879−2887.
6. Pickhardt, M., Gazova, Z., von Bergen, M., Khlistunova, I., Wang, Y., Hascher, A., Mandelkow, E. M., Biernat, J., and Mandelkow, E. (2005) Anthraquinones inhibit tau aggregation and dissolve alzheimer paired helical filaments in vitro and in cells, *J. Biol. Chem. 280*, 3628−3635.
7. Taniguchi, S., Suzuki, N., Masuda, M., Hisanaga, S., Iwatsubo, T., Goedert, M., and Hasegawa, M. (2005) Inhibition of heparin-induced tau filament formation by phenothiazines, polyphenols, and porphyrins, *J. Biol. Chem. 280*, 7614−7623.
8. Wilson, D. M., and Binder, L. I. (1997) Free fatty acids stimulate the polymerization of tau and amyloid β peptides. In vitro evidence for a common effector of pathogenesis in Alzheimer's disease, *Am. J. Pathol. 150*, 2181−2195.
9. Chirita, C. N., Necula, M., and Kuret, J. (2003) Anionic micelles and vesicles induce tau fibrillization in vitro, *J. Biol. Chem. 278*, 25644−25650.
10. Chirita, C. N., and Kuret, J. (2004) Evidence for an intermediate in tau filament formation, *Biochemistry 43*, 1704−1714.
11. Perez, M., Valpuesta, J. M., Medina, M., Montejo de Garcini, E., and Avila, J. (1996) Polymerization of tau into filaments in the presence of heparin: The minimal sequence required for tau−tau interaction, *J. Neurochem. 67*, 1183−1190.
12. Kampers, T., Friedhoff, P., Biernat, J., Mandelkow, E. M., and Mandelkow, E. (1996) RNA stimulates aggregation of microtubule-associated protein tau into Alzheimer-like paired helical filaments, *FEBS Lett. 399*, 344−349.
13. Hasegawa, M., Crowther, R. A., Jakes, R., and Goedert, M. (1997) Alzheimer-like changes in microtubule-associated protein Tau induced by sulfated glycosaminoglycans. Inhibition of microtubule binding, stimulation of phosphorylation, and filament assembly depend on the degree of sulfation, *J. Biol. Chem. 272*, 33118−33124.
14. Kuret, J., Chirita, C. N., Congdon, E. E., Kannanayakal, T., Li, G., Necula, M., Yin, H., and Zhong, Q. (2005) Pathways of tau fibrillization, *Biochim. Biophys. Acta 1739*, 167−178.
15. Randolph, A. D., and Larson, M. A. (1988) *Theory of Particulate Processes: Analysis and Techniques of Continuous Crystallization*, Academic Press, San Diego.
16. Chirita, C. N., Congdon, E. E., Yin, H., and Kuret, J. (2005) Triggers of full-length tau aggregation: A role for partially folded intermediates, *Biochemistry 44*, 5862−5872.
17. Timasheff, S. N. (1981) The Self-Assembly of Long Rodlike Structures, in *Protein−Protein Interactions* (Nichol, L. W., Ed.) pp 315−336, John Wiley and Sons, New York.
18. King, M. E., Ahuja, V., Binder, L. I., and Kuret, J. (1999) Ligand-dependent tau filament formation: Implications for Alzheimer's disease progression, *Biochemistry 38*, 14851−14859.
19. King, M. E., Ghoshal, N., Wall, J. S., Binder, L. I., and Ksiezak-Reding, H. (2001) Structural analysis of Pick's disease-derived and in vitro-assembled tau filaments, *Am. J. Pathol. 158*, 1481−1490.
20. Necula, M., and Kuret, J. (2004) A static laser light scattering assay for surfactant-induced tau fibrillization, *Anal. Biochem. 333*, 205−215.
21. Necula, M., and Kuret, J. (2004) Pseudophosphorylation and glycation of tau protein enhance but do not trigger fibrillization in vitro, *J. Biol. Chem. 279*, 49694−49703.
22. Augustinack, J. C., Schneider, A., Mandelkow, E. M., and Hyman, B. T. (2002) Specific tau phosphorylation sites correlate with severity of neuronal cytopathology in Alzheimer's disease, *Acta Neuropathol. 103*, 26−35.
23. Kimura, T., Ono, T., Takamatsu, J., Yamamoto, H., Ikegami, K., Kondo, A., Hasegawa, M., Ihara, Y., Miyamoto, E., and Miyakawa, T. (1996) Sequential changes of tau-site-specific phosphorylation during development of paired helical filaments, *Dementia 7*, 177−181.
24. Smith, M. A., Tabaton, M., and Perry, G. (1996) Early contribution of oxidative glycation in Alzheimer's disease, *Neurosci. Lett. 217*, 210−211.
25. Carmel, G., Mager, E. M., Binder, L. I., and Kuret, J. (1996) The structural basis of monoclonal antibody Alz50's selectivity for Alzheimer's disease pathology, *J. Biol. Chem. 271*, 32789−32795.
26. Bruns, G., and Beerhalter, H. (1955) Dye analysis. The fluorochrome mixture, thioflavine S, *Acta Histochem. 1*, 254−271.
27. Necula, M., and Kuret, J. (2004) Electron microscopy as a quantitative assay for studying tau fibrillization, *Anal. Biochem. 329*, 238−246.
28. Gamblin, T. C., King, M. E., Dawson, H., Vitek, M. P., Kuret, J., Berry, R. W., and Binder, L. I. (2000) In vitro polymerization of tau protein monitored by laser light scattering: Method and application to the study of FTDP-17 mutants, *Biochemistry 39*, 6136−6144.
29. West, W., and Pearce, S. (1965) The dimeric state of cyanine dyes, *J. Phys. Chem. 69*, 1894−1903.

30. Evans, K. C., Berger, E. P., Cho, C. G., Weisgraber, K. H., and Lansbury, P. T., Jr. (1995) Apolipoprotein E is a kinetic but not a thermodynamic inhibitor of amyloid formation: Implications for the pathogenesis and treatment of Alzheimer disease, *Proc. Natl. Acad. Sci. U.S.A. 92*, 763−767.
31. Cheng, H. C. (2004) The influence of cooperativity on the determination of dissociation constants: Examination of the Cheng-Prusoff equation, the Scatchard analysis, the Schild analysis and related power equations, *Pharmacol. Res. 50*, 21−40.
32. Kashchiev, D. (2000) *Nucleation: Basic theory with applications*, Butterworth Heinemann, Oxford, U.K.
33. Zhao, D., and Moore, J. S. (2003) Nucleation-elongation: A mechanism for cooperative supramolecular polymerization, *Org. Biomol. Chem. 1*, 3471−3491.
34. Necula, M., and Kuret, J. (2005) Site-specific pseudophosphorylation modulates the rate of tau filament dissociation, *FEBS Lett. 579*, 1453−1457.
35. Craig, D. A. (1993) The Cheng-Prusoff relationship: Something lost in the translation, *Trends Pharmacol. Sci. 14*, 89−91.
36. Friedhoff, P., Schneider, A., Mandelkow, E. M., and Mandelkow, E. (1998) Rapid assembly of Alzheimer-like paired helical filaments from microtubule-associated protein tau monitored by fluorescence in solution, *Biochemistry 37*, 10223−10230.
37. Dahlquist, F. W. (1978) The meaning of Scatchard and Hill plots, *Methods Enzymol. 48*, 270−299.
38. Ben-Naim, A. (2001) *Cooperativity and Regulation in Biochemical Processes*, Kluwer Academic Publishers, New York.
39. Herz, A. H. (1977) Aggregation of sensitizing dyes in solution and their adsorption on to silver halides, *Adv. Colloid Interface Sci. 8*, 237−298.
40. Maskasky, J. E. (1991) Molecular-orientation of individual J aggregates on gelatin-grown AgBr tabular microcrystals, *Langmuir 7*, 407−421.
41. Harrison, W. J., Mateer, D. L., and Tiddy, G. J. T. (1996) Liquid-crystalline J-aggregates formed by aqueous ionic cyanine dyes, *J. Phys. Chem. 100*, 2310−2321.
42. Seifert, J. L., Connor, R. E., Kushon, S. A., Wang, M., and Armitage, B. A. (1999) Spontaneous assembly of helical cyanine dye aggregates on DNA nanotemplates, *J. Am. Chem. Soc. 121*, 2987−2995.
43. Stryer, L., and Blout, E. R. (1961) Optical rotatory dispersion of dyes bound to macromolecules. Cationic dyes: Polyglutamic acid complexes, *J. Am. Chem. Soc. 83*, 1411−1418.
44. Hermel, H., Holtje, H. D., Bergemann, S., De Rossi, U., and Kriwanek, J. (1995) Band-shifting through polypeptide β-sheet structures in the cyanine UV−vis spectrum, *Biochim. Biophys. Acta 1252*, 79−86.
45. Hermel, H., Schmahl, W., and Mohwald, H. (1999) Selective staining by the fluorochrome, 5,5-diphenyl-9-ethyl-$DiOC_2$(3). I. Physicochemical studies of dye-dye and dye-tissue interactions, *Biotech. Histochem. 74*, 221−228.
46. Sabate, R., and Estelrich, J. (2003) Pinacyanol as effective probe of fibrillar β-amyloid peptide: Comparative study with Congo Red, *Biopolymers 72*, 455−463.
47. Friedhoff, P., von Bergen, M., Mandelkow, E. M., Davies, P., and Mandelkow, E. (1998) A nucleated assembly mechanism of Alzheimer paired helical filaments, *Proc. Natl. Acad. Sci. U.S.A. 95*, 15712−15717.
48. Sciarretta, K. L., Gordon, D. J., Petkova, A. T., Tycko, R., and Meredith, S. C. (2005) Aβ40-Lactam(D23/K28) Models a Conformation Highly Favorable for Nucleation of Amyloid, *Biochemistry 44*, 6003−6014.
49. Gray, E. G., Paula-Barbosa, M., and Roher, A. (1987) Alzheimer's disease: Paired helical filaments and cytomembranes, *Neuropathol. Appl. Neurobiol. 13*, 91−110.
50. Zhu, M., Souillac, P. O., Ionescu-Zanetti, C., Carter, S. A., and Fink, A. L. (2002) Surface-catalyzed amyloid fibril formation, *J. Biol. Chem. 277*, 50914−50922.
51. Barghorn, S., and Mandelkow, E. (2002) Toward a unified scheme for the aggregation of tau into Alzheimer paired helical filaments, *Biochemistry 41*, 14885−14896.
52. Gamblin, T. C., King, M. E., Kuret, J., Berry, R. W., and Binder, L. I. (2000) Oxidative regulation of fatty acid-induced tau polymerization, *Biochemistry 39*, 14203−14210.
53. Li, J., Zhu, M., Rajamani, S., Uversky, V. N., and Fink, A. L. (2004) Rifampicin inhibits α-synuclein fibrillation and disaggregates fibrils, *Chem. Biol. 11*, 1513−1521.
54. Zhu, M., Rajamani, S., Kaylor, J., Han, S., Zhou, F., and Fink, A. L. (2004) The flavonoid baicalein inhibits fibrillation of α-synuclein and disaggregates existing fibrils, *J. Biol. Chem. 279*, 26846−26857.
55. Conway, K. A., Rochet, J. C., Bieganski, R. M., and Lansbury, P. T., Jr. (2001) Kinetic stabilization of the α-synuclein protofibril by a dopamine-α-synuclein adduct, *Science 294*, 1346−1349.
56. LeVine, H., III (1993) Thioflavine T interaction with synthetic Alzheimer's disease β-amyloid peptides: Detection of amyloid aggregation in solution, *Protein Sci. 2*, 404−410.
57. LeVine, H., III (1999) Quantification of β-sheet amyloid fibril structures with thioflavin T, *Methods Enzymol. 309*, 274−284.
58. Carter, D. B., and Chou, K. C. (1998) A model for structure-dependent binding of Congo red to Alzheimer β-amyloid fibrils, *Neurobiol. Aging 19*, 37−40.
59. Jin, L. W., Claborn, K. A., Kurimoto, M., Geday, M. A., Maezawa, I., Sohraby, F., Estrada, M., Kaminksy, W., and Kahr, B. (2003) Imaging linear birefringence and dichroism in cerebral amyloid pathologies, *Proc. Natl. Acad. Sci. U.S.A. 100*, 15294−15298.
60. Krebs, M. R., Bromley, E. H., and Donald, A. M. (2005) The binding of thioflavin-T to amyloid fibrils: Localisation and implications, *J. Struct. Biol. 149*, 30−37.
61. Kim, Y. S., Randolph, T. W., Manning, M. C., Stevens, F. J., and Carpenter, J. F. (2003) Congo red populates partially unfolded states of an amyloidogenic protein to enhance aggregation and amyloid fibril formation, *J. Biol. Chem. 278*, 10842−10850.
62. Khurana, R., Uversky, V. N., Nielsen, L., and Fink, A. L. (2001) Is Congo red an amyloid-specific dye? *J. Biol. Chem. 276*, 22715−22721.
63. Murakami, K. (2002) Thermodynamic and kinetic aspects of self-association of dyes in aqueous solution, *Dyes Pigm. 53*, 31−43.
64. McGovern, S. L., Caselli, E., Grigorieff, N., and Shoichet, B. K. (2002) A common mechanism underlying promiscuous inhibitors from virtual and high-throughput screening, *J. Med. Chem. 45*, 1712−1722.
65. Liu, H. Y., Wang, Z., Regni, C., Zou, X., and Tipton, P. A. (2004) Detailed kinetic studies of an aggregating inhibitor; Inhibition of phosphomannomutase/phosphoglucomutase by disperse blue 56, *Biochemistry 43*, 8662−8669.
66. Mishra, A., Behera, R. K., Behera, P. K., Mishra, B. K., and Behera, G. B. (2000) Cyanines during the 1990s: A review, *Chem. Rev. 100*, 1973−2011.
67. Garoff, R. A., Litzinger, E. A., Connor, R. E., Fishman, I., and Armitage, B. A. (2002) Helical aggregation of cyanine dyes on DNA templates: Effect of dye structure on formation of homo- and heteroaggregates, *Langmuir 18*, 6330−6337.
68. Turner, P. R., and Denny, W. A. (2000) The genome as a drug target: Sequence specific minor groove binding ligands, *Curr. Drug Targets 1*, 1−14.
69. Sima, P. D., and Kanofsky, J. R. (2000) Cyanine dyes as protectors of K562 cells from photosensitized cell damage, *Photochem. Photobiol. 71*, 413−421.
70. Caesar, J., Shaldon, S., Chiandussi, L., Guevara, L., and Sherlock, S. (1961) The use of indocyanine green in the measurement of hepatic blood flow and as a test of hepatic function, *Clin. Sci. 21*, 43−57.
71. Brancato, R., and Trabucchi, G. (1998) Fluorescein and indocyanine green angiography in vascular chorioretinal diseases, *Semin. Ophthalmol. 13*, 189−198.
72. Ko, L. W., DeTure, M., Sahara, N., Chihab, R., Vega, I. E., and Yen, S. H. (2005) Recent advances in experimental modeling of the assembly of tau filaments, *Biochim. Biophys. Acta 1739*, 125−139.
73. DeTure, M., Ko, L., Easson, C., Hutton, M., and Yen, S. H. (2001) Inducible transgenic expression of wild-type tau in H4 neuroglioma cells, in *Alzheimer's Disease: Advances in Etiology, Pathogenesis and Therapeutics* (Iqbal, K., Sisodia, S. S., and Winblad, B., Eds.) pp 651−660, Wiley, Chichester, U.K.
74. Hyman, B. T., Augustinack, J. C., and Ingelsson, M. (2005) Transcriptional and conformational changes of the tau molecule in Alzheimer's disease, *Biochim. Biophys. Acta 1739*, 150−157.
75. Yasojima, K., McGeer, E. G., and McGeer, P. L. (1999) Tangled areas of Alzheimer brain have upregulated levels of exon 10 containing tau mRNA, *Brain Res. 831*, 301−305.
76. Geerts, H. (2004) NC-531, *Curr. Opin. Invest. Drugs 5*, 95−100.
77. Pollack, S. J., Sadler, I. I. J., Hawtin, S. R., Tailor, V. J., and Shearman, M. S. (1995) Sulfonated dyes attenuate the toxic effects of β-amyloid in a structure-specific fashion, *Neurosci. Lett. 197*, 211−214.

78. Tint, I., Slaughter, T., Fischer, I., and Black, M. M. (1998) Acute inactivation of tau has no effect on dynamics of microtubules in growing axons of cultured sympathetic neurons, *J. Neurosci. 18*, 8660−8673.
79. Harada, A., Oguchi, K., Okabe, S., Kuno, J., Terada, S., Ohshima, T., Sato-Yoshitake, R., Takei, Y., Noda, T., and Hirokawa, N. (1994) Altered microtubule organization in small-calibre axons of mice lacking tau protein, *Nature 369*, 488−491.
80. Ikegami, S., Harada, A., and Hirokawa, N. (2000) Muscle weakness, hyperactivity, and impairment in fear conditioning in tau-deficient mice, *Neurosci. Lett. 279*, 129−132.
81. Heiser, V., Engemann, S., Brocker, W., Dunkel, I., Boeddrich, A., Waelter, S., Nordhoff, E., Lurz, R., Schugardt, N., Rautenberg, S., Herhaus, C., Barnickel, G., Bottcher, H., Lehrach, H., and Wanker, E. E. (2002) Identification of benzothiazoles as potential polyglutamine aggregation inhibitors of Huntington's disease by using an automated filter retardation assay, *Proc. Natl. Acad. Sci. U.S.A. 99*, 16400−16406.
82. Blanchard, B. J., Chen, A., Rozeboom, L. M., Stafford, K. A., Weigele, P., and Ingram, V. M. (2004) Efficient reversal of Alzheimer's disease fibril formation and elimination of neurotoxicity by a small molecule, *Proc. Natl. Acad. Sci. U.S.A. 101*, 14326−14332.
83. Gestwicki, J. E., Crabtree, G. R., and Graef, I. A. (2004) Harnessing chaperones to generate small-molecule inhibitors of amyloid β aggregation, *Science 306*, 865−869.
84. Masel, J., and Jansen, V. A. (2000) Designing drugs to stop the formation of prion aggregates and other amyloids, *Biophys. Chem. 88*, 47−59.
85. Hammarstrom, P., Wiseman, R. L., Powers, E. T., and Kelly, J. W. (2003) Prevention of transthyretin amyloid disease by changing protein misfolding energetics, *Science 299*, 713−716.

BI050387O